Journal of Intelligent Systems and Internet of Things
Vol. 13, No. 01, PP. 135-150, 2024
DOI: https://doi.org/10.54216/JISIoT.130111

Fractal Dimension on CBCT Images and Modular Neural Networks to Identify Reduced Bone Mineral Density in Women

Eman Shawky Mira[1], Ahmed Mohamed Saaduddin Sapri [1,2], Taseer Bashir[3,4] , Khalid Hassan[5], Abdulhameed Saeed Alghamdi[6], Yousef Almasaabi[6] , Nagham Talal Maddah[6] , Hind F. Kayal[6], El-Sayed M. El-kenawy[7,*], Mohamed Saber[8]

[1]Faculty of Dentistry, Mansoura University, Mansoura 35516, Egypt; [2]Dentistry Program, Clinical Dental Science Department, Division of Oral and Maxillofacial Surgery, Batterjee Medical College, Jeddah, 21442, Saudi Arabia; [3]Dentistry Program, Oral Medicine and Radiology Department, Batterjee Medical College, Jeddah, 21442, Saudi Arabia; [4]PhD Candidate, Teerthankar Mahaveer Dental College, Moradabad, India [5]Radiologic Science Program, Batterjee Medical College, Makkah Region, Jeddah, 21442, Saudi Arabia; [6] Intership Dentist, Dental Clinics of Batterjee Medical College, Jeddah, Makka Region, 21442, Saudi Arabia; [7] Department of Communications and Electronics, Delta Higher Institute of Engineering and Technology, Mansoura, 3511, Egypt; [8]Electronics and Communications Engineering Department, Faculty of Engineering, Delta University for Science and Technology, Gamasa City, 11152, Egypt

Emails: emanshawky@mans.edu.eg; ahmedsaaduddin@mans.edu.eg; taseer.bashir@bmc.edu.sa; khalid.hassan28@gmail.com; Abdulhameed-17@hotmail.com; y.almasaabi97@gmail.com; Naghammaddah1998@gmail.com; hindkayal.hk@gmail.com; skenawy@ieee.org; Mohamed.Saber@deltauniv.edu.eg

Abstract

This paper provides two different methods to diagnose osteoporosis in women; the first method is the fractal analysis evaluated by CBCT at two bone locations (the mandible and the second cervical vertebrae) to see if there is any correlation between the two. At the same time, the second method is deep convolutional neural networks (DCNNs). One hundred eighty-eight patients' mandibular CBCT images were used, and DCNN models based on the ResNet-101 framework were employed. Dual X-ray absorptiometry of the hip and lumbar spine revealed that 139 of the 188 postmenopausal women tested had osteoporosis, whereas 49 had average bone mineral density. The second cervical vertebra and the mandible were selected as locations of interest for FD analysis on the CBCT images. Measurement accuracy, both within and between observers' agreements, and correlations between two data sets were all calculated. To evaluate osteoporosis, we used a segmented, three-phase approach. Stage 1 was devoted to the identification of mandibular bone slices. In Stage 2, the coordinates for the mandible's cross-sectional views were established, and Stage 3 calculated the thickness of the mandible bone, emphasizing osteoporotic variations. The average FD values within the interest area of the mandible were significantly lower in people with osteoporosis than in those with average bone mineral density. At the same time, the two groups had no significant difference in FD values at the second cervical vertebra. For the mandibular site, areas beneath the curve were 0.644 ($P = 0.008$), while the area under the curve for the vertebral site was 0.531 ($P = 0.720$). DCNN training in the first stage yielded an astounding 98.85% training accuracy, the second stage decreased L1 loss to a meager 1.02 pixels, and the bone thickness computation method used in the last stage had a mean squared error of 0. 8377. We concluded that FD was underutilized even though it distinguished between women with normal BMD and those with osteoporosis in the mandibular area. Additionally, even with small mandibular CBCT datasets, the results show the value of a modular transfer learning approach for osteoporosis detection.

Received: September 02, 2023 Revised: December 19, 2023 Accepted: June 02, 2024

Keywords: Osteoporosis; Cone-Beam Computed Tomography; Fractals; Dual-Energy X-ray Absorptiometry; deep convolutional neural networks (DCNNs).

1. Introduction

Osteoporosis is a common skeletal disease that weakens bones and increases susceptibility to fractures from relatively minor injuries. Fragility fractures are another name for these types of breaks. Bone quality and bone mineral density (BMD) are the most crucial factors influencing bone strength [1]. The social and economic cost of fragility fractures makes osteoporosis a significant issue for public health. This disorder is most common among the elderly and among women who have gone through menopause. The aging of the affected population has a historical tendency to increase the associated costs. Low bone mineral density increases the risk of fractures; hence, it is crucial to identify people with this condition [2-4]. Bone mineral density (BMD) measurements utilizing dual-energy X-ray absorption spectroscopy (DXA) are the gold standard for diagnosing osteoporosis. Despite DXA's status as the diagnostic gold standard for osteoporosis, the test is not widely available and has certain limitations when gauging quality of life.

The social and economic cost of fragility fractures makes osteoporosis a significant issue for public health. This disorder is most common among the elderly and among women who have gone through menopause. The aging of the affected population has a historical tendency to increase the associated costs. CBCT scans' fractal dimension analysis to find decreased bone mineral density in women who have gone through menopause has limited utility. Despite DXA's status as the benchmark for osteoporosis diagnosis, the test is not publicly accessible [5]. Patients with average bone mineral density (BMD) or osteopenia, as measured by DXA, are not immune to fragility fractures [6]. This means that additional tests are needed to recognize alterations in the microstructure of bone. The microstructure's complexity is one of the most essential elements determining the bones' strength [7].

Several authors have proposed a link between bone microarchitecture and the study of picture texture and gray value in radiography [8,9]. When paired with bone mineral density, fractal dimension (FD) analysis of the femur and vertebrae are examples of bone texture imaging characteristics that could improve failure load prediction [10–12]. A mathematical method called FD makes it possible to quantify complex structures in a way that is not attainable with more standard mathematics methods. This method assesses the degree to which irregularities and forms are present in the researched objects. The complexity of the image has a direct influence on the value that it carries [13]. Although FD in dental imaging modalities has been investigated as an additional method to identify people with low BMD, most research has relied on conventional, two-dimensional assessments. Cone-beam computed tomography, or CBCT, scans are becoming more and more common in dental offices between the ages of 45 and 70 [14-19]. The aged population is at the most risk for developing osteoporosis. Hence, CBCT scans are routinely used for various reasons, including the planning of implants, the detection of areas with illness, and the localization of retained teeth [20,21]. Recent research on CBCT indices has been limited, but what there is suggests that it could be helpful in screening for osteoporosis [22-25]. Only two studies in recent years have looked into FD evaluation with CBCT to identify ladies who have post-menopause and osteoporosis, and their findings don't match up [26,27]. However, these investigations utilized a fundamentally different technique, had extremely tiny samples, and were entirely observational. As a result, not a single study established accuracy measurements for the FD approach.

The application of artificial intelligence (AI) has the potential to revolutionize medical diagnostics by enhancing scalability, accuracy, and efficiency. Artificial Intelligence is frequently utilized in medical diagnostics to analyze imaging data, such as CT, MRI, and X-ray scans. Deep learning algorithms can precisely recognize patterns and features in medical images to help with the early detection and diagnosis of diseases, including lung cancer [28]. AI can assess patient data, including test results, vital signs, and EHRs in medical diagnostics. AI systems combine NLP and ML. Artificial intelligence (AI) can assess patient data, including test results and vital signs, and electronic health records in the context of medical diagnosis. AI systems integrate ML and NLP.

AI has drawbacks, even if it can potentially transform medical diagnostics. AI systems need large amounts of high-quality data for training, which might be challenging. Bias in training data could result in incorrect predictions. Interpretation becomes challenging due to the complexity of understanding how AI models arrive at their results. While AI can potentially lower healthcare expenses and improve medical diagnoses, further research is required to address its limitations. AI must be applied morally and sensibly [29]. With sensitivity and specificity values above 70%, studies show that mandibular assessments of fractal dimensions are a valid biomarker for osteoporosis screening. Specificity was not as functional as osteoporosis screening [30]. To examine each one's performance, this study presents two methods: the first uses fractal analysis of CBCT images. Cone-beam computed tomography (CBCT) scans of the mandible can be used to identify osteoporotic changes using deep convolutional neural networks (DCNNs), which are based on the ResNet-101 architecture [31]. Machine learning is being used in this novel method of osteoporosis detection to increase explainability and diagnostic efficacy.

This study distinguishes itself by employing a three-stage modular methodology. Every stage improves the diagnostic system's efficiency and fulfills a specific purpose. The system's explain-ability and DCNN training are enhanced by using modular tasks that are functionally isolated from one another. Even with few datasets, this innovative technique accurately detects osteoporosis in mandibular CBCT images through a modular transfer learning mechanism. This research aims to design and evaluate a deep neural network for osteoporosis risk assessment using maxillofacial CBCT scans.

2. Materials and Methods

One hundred twenty individuals were first selected from the service for Bone Densitometry database at the University Hospital of Mansoura. BMD was either normal or indicating osteopenia or osteoporosis. Since 20 patients were determined to have osteopenia and be disqualified for the experiment, only 100 were considered for participation. This criterion for exclusion was chosen so that we could ignore information on the borderline between normal BMD and osteoporosis. The densities of the lumbar and hip bone tests obtained from the selected individuals led to the diagnosis of osteoporosis in 139 patients, as revealed by DEXA measurements.

In contrast, the remaining 49 patients had average bone mineral density (BMD). In addition to being 45 or older and having gone through menopause, potential participants had to obtain CBCT scans for the implant scheme. Individuals who had used medications that affected bone metabolism or had previously been diagnosed with other metabolic bone problems were not eligible to participate in the trial. Postmenopausal women with missing teeth or who had all extracted made for a good sample because they were all candidates for CBCT scans for implant site assessment. There was a maximum three-month gap between the DXA and the CBCT. The study met all of the ethical requirements set forth by the institutional research committee at the faculty of dentistry at Mansoura University. The study obtained ethical approval for scientific research with the specific number (A01010023OM). Every person who took part in the research project was given and had to sign an "informed consent" form. T and F values in a distribution of 0.99 (effect size = 0.3 and type I error = 0.05) show enough participants in the study to achieve statistical significance.

2.1 BMD assessment

The same technician performed DXA scans on the hip and lumbar spine (L1-L4) using a Lunar DPX NT instrument. The World Health Organization's guidelines for bone mineral density were used to classify the results for the lumbar spine, femoral neck (FN), and total hip (TH) as either normal (T-score ≥-1.0) or osteoporosis (T-score -≤2.5). Patients were diagnosed with osteoporosis based on these results. Suppose the T-scores for any of the regions above were compatible. The coefficients of variance for a subset of hip and lumbar spine measures were 1.2% and 1%, respectively.

A. Fractal Analysis of CBCT scans

Patients who needed to make CBCT scans for the mandible for implant purposes were involved in the study. To acquire CBCT images, an I-CAT Classic machine was used with the following settings: 0.25 mm voxel size, 120 kV, 8 mA, 20 cm 8 cm field of view, and 40 seconds for each scan. The noise known about image formation of CBCT images was controlled firstly before patient exposure by proper calibrations of both the CBCT machine and detectors. Secondly, I performed the measurements on high-resolution images with a small voxel size (0.25mm). Thirdly, after processing, we used median filters provided by Image J software that made image smoothening.

The manufacturer-supplied software for the CBCT was used to do the initial analysis of the images. Two areas of concern were chosen from the CBCT pictures' output. Previous studies were consulted for their recommendations on the optimal size and form of the areas of interest. The first ROI (region of interest) (ROI-v) evaluated the second cervical vertebra (C2) using 0.25 mm slices, while the second ROI (ROI-m) in the mandible (ROI-m) employed 1.25 mm slices. The images were examined in axial, sagittal, and coronal sections.

The criteria for selecting CBCT cuts were used using the multiplanar reformation screen. Axial images with a slice thickness of 0.1 mm were selected, and the mental foramen was identified by scrolling through sequential slices. The slice that identified and represented the widest mesiodistal dimension of the mental foramen was selected 8. The ROI-v was obtained using the C2 coronal view. According to Figures 1(a), 1(b), and 1(c), the centroid of C2 was used to select this ROI in the sagittal, axial, and coronal planes, respectively.

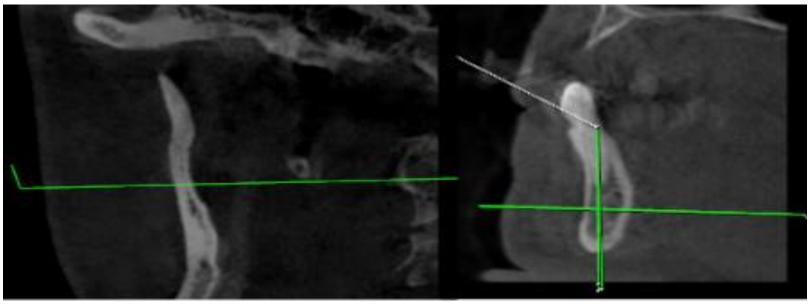

(a)

(b)

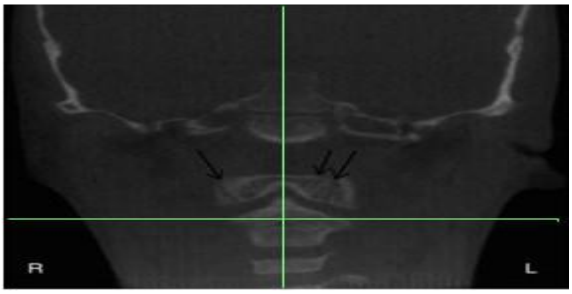

(c)

Figure 1: slices used to evaluate the locations and alignments of the second cervical vertebra (C2). A constructed line tilts the sagittal plane (a) perpendicular to the computer screen and passes through the dens. A cross designates the center of the dens, found in both the axial (b) and coronal (c) scans.

Then, using the axial figure 2(a) and reconstructed panoramic image figure 2 (b) planes, the region of interest (ROI) was defined. The panoramic reconstruction image in Figure 2(b) shows only trabecular bone, with no cortical bone evident in the overlap.

The right side of the jaw was selected as the region of interest (ROI). This choice ensured that teeth, foramina, and the inferior alveolar canal wouldn't get in the way. Specific individuals with posterior edentulous regions have a higher chance of having a smaller bone volume due to physiological remodeling, which is another benefit of this posture. The regions of interest for the cervical spine (Figure 1(c)) and mandible (Figure 2(b) were each 40 pixels by 40 pixels in size.

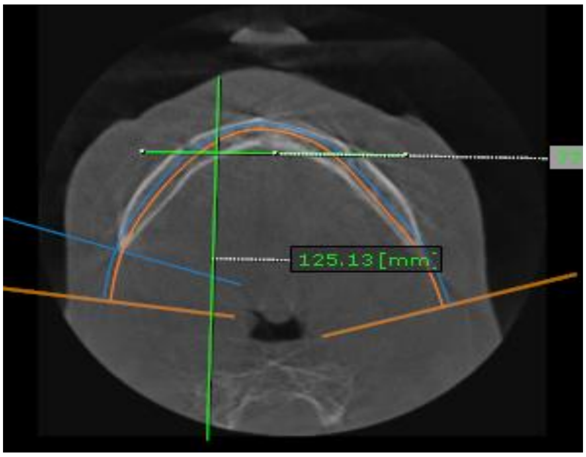

(a)

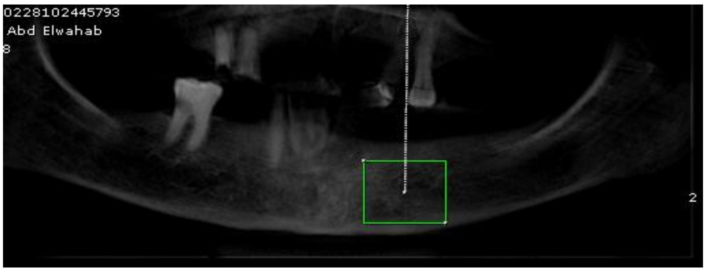

(b)

Figure 2: demonstrates the positions and alignments of the slices utilized to evaluate the mandible. (a) The cutting curve is drawn at the right-side corner of the mandible's axial picture to reconstruct the panoramic image. (b) The Standardization is to minimize any cortical bone overlap and highlight the appearance of trabecular bone. A region of interest of 40 by 40 pixels was chosen for the mandibular site.

The analysis of FD was performed with the help of the Bone J plugin for ImageJ. The box-counting technique is used in this extension. After processing the images, FD was determined using the standard approach detailed by White and Rudolph (1999) for evaluating conventional radiographs14-16. References to these studies can be found throughout this paragraph [32]. Since CBCT records information in three dimensions, this image processing method was adapted for use with CBCT. The stages involved in applying this method to the selected ROIs are as follows. They are depicted in Figure 3: figure 3(a) shows the ROI being copied, followed by the application of a 10-pixel Gaussian filter figure (3b) to take out the medium and delicate structures, leaving only significant variations in density figure (3c), followed by the transformation of this picture into an 8-bit binary image. Figure (3d), and finally, the outlining and skeletonization of the trabeculae figure 3(e), figure 3(f).

(a) (b) (c)

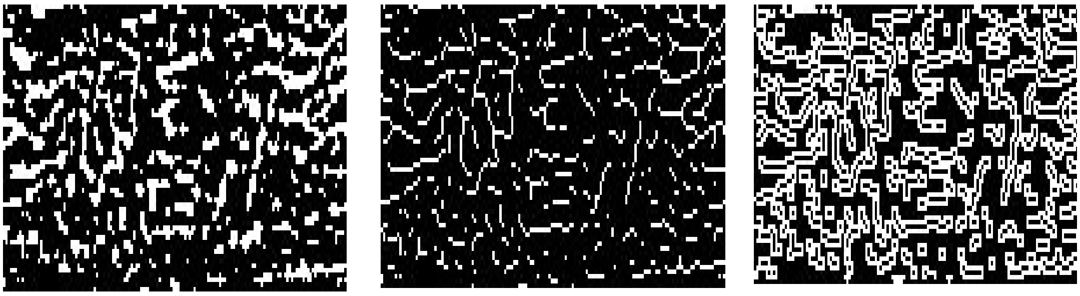

(d) (e) (f)

Figure 3: Fractal dimension analysis image processing technique. a. Duplication. c. A 10.00-pixel Gaussian filter. c. Deducting the second picture from the initial one. d. The picture is transformed into an 8-bit binary image. e. Deboned structure (skeletonization). f. the trabeculae of the bones are outlined.

FD analysis is also depicted graphically in this image in Figure 4. We got two separate FD measurements, one for each ROI. The photos were viewed on an LCD panel with a resolution of 1280 by 1024 in a poorly lit room. The same observer did two separate FD examinations within a week of each other to determine intra-observer reliability. Inter-observer reliability was calculated by comparing the analyses performed by two independent observers. Two oral and maxillofacial radiologists supervised CBCT scans, each with more than four years of experience in their field. Neither of the watchers had seen the DXA results. Table 1 indicates the measured box size counting in the image.

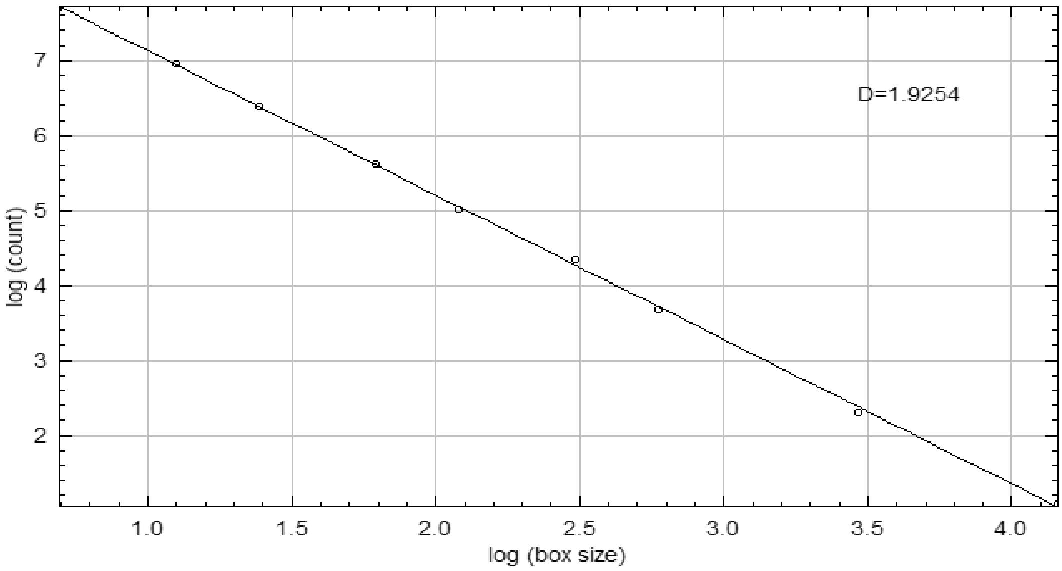

Figure 4: A Graph Represents the Box-Counting Procedure and Calculation.

Table 1: The Image J Program Measured Box Size Counting.

Box	Count
2	2240
3	1049
4	592
6	275
8	152
12	78
16	40
32	10
64	3

2.2 Modular Neural Network

Using the technique outlined by Koh et al. [33], the Dental Module system's multi-planar reconstruction (MPR) view produced a modified parasagittal image of the mandible. The condition of the mandible's cortical bone structure distal from the mental foramen in the obtained parasagittal image was used to calculate the computed tomography cortical index (CTCI), which was divided into three groups [34], as seen in Figure 5:

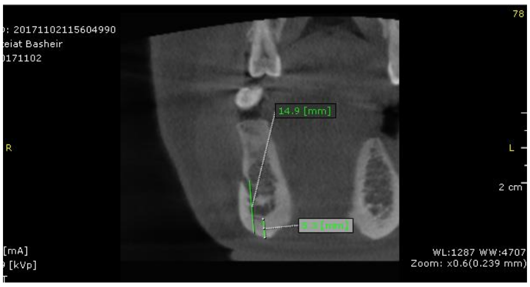

(a)

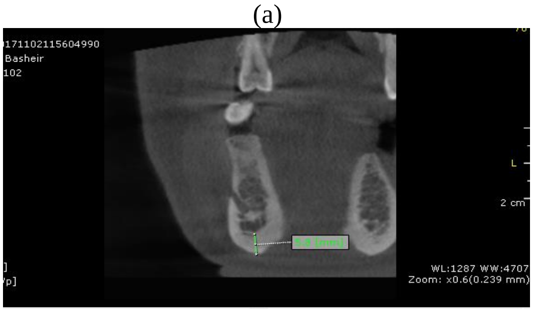

(b)

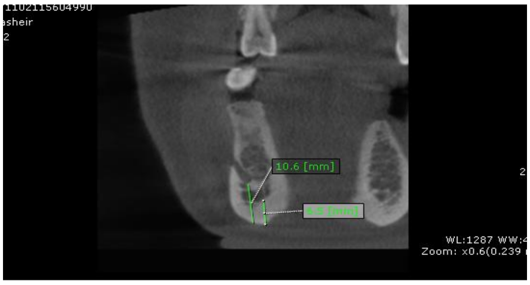

(c)

Figure 5: Computed cortical index on tomography. The cortex's endosteal edge is smooth and crisp in (a) C1, semilunar defects or one to two resorption lacunae are seen in (b) C2, and the cortical layer developed substantial endosteal residues and was porous in (c) (C3).

A. Modular Neural Network:

The modular neural network, an integrated system of two fundamental neural networks built on the ResNet-101 architecture, is the central component of the methodology. ResNet-101, with its 101 levels of depth, is well-known. Its key strength is deep residual learning, which effectively solves the vanishing gradient problem. The unique 1 * 1 convolution layers and 3 * 3-pixel filters of the architecture improve performance. A more thorough function representation with fewer parameters is possible when average pooling layers are used instead of fully linked ones.

B. Pre-processing of Data:

1. **Data Acquisition**: The NRRD file format, a standard for storing multidimensional data like CT images, was first used to acquire the data.
2. **Data Conversion**: These NRRD files were transformed into a numpy container format to improve compatibility and processing ease, making them more appropriate for neural networks and data manipulation.
3. **Normalization**: Normalization was done to consider the inherent heterogeneity in radiological data. This stage redistributed values inside each volume to provide uniformity and help the neural network recognize patterns more successfully, setting the minimum and maximum values to -0.5 and 0.5, respectively.

4. **Labeling:** Manual labeling, a vital step, has been performed. Experts accurately recognized and designated the slice in the axial plane, ensuring that both foramina mental were visible.

ResNet-101 First Classification Network:

1. **Network Initialization:** Random weights and biases were set up in a neural network constructed on the ResNet-101 design**.**
2. **Training:** The network underwent supervised training with the labeled dataset to fine-tune its weights and biases**.**
3. **Output Analysis:** The network's capacity to classify slices into "yes" (mandibular bone present) and "no" was demonstrated in the post-training scenario. A probability value representing the network's confidence level in each classification was provided.
4. **Weight Storage:** Every weight acquired throughout the training was painstakingly documented in a different digital file to guarantee uniformity and avoid retraining.
5. **Validation:** After training, a second validation set assessed the model's performance. Essential features like precision, accuracy, and recall were used to evaluate the model's robustness**.**
6. **image data processing:** The network was supplied with an extensive image dataset. The network calculated and allocated a probability coefficient to each slice, signifying the possibility of the slice holding the mandibular bone**.**
7. **Identification of Optimal Slice:** The probability coefficients were sorted using an analytical method. The slice with the most outstanding value was chosen and marked for further study.

In the first step, we use the ResNet-101 neural network model to tackle a classification task. The ResNet-101 model was obtained from the official PyTorch library. The last layer of the ResNet-101 model was modified to achieve the desired outcomes. Two categories were created out of the data: "correct slice" and "incorrect slice." At this point, the objective is to use M RI digital pictures to locate the appropriate jaw slice. Before selecting the vertical slice that represents the jaw, the neural network examines all of them. Moving through the phases, this slice becomes essential for making an orthogonal cut in a specific jaw location. Cuts that reveal the jaw are considered authentic and are standard for the next stage. We extracted the slice with the highest likelihood.

Regarding model modifications, we included a new convolutional layer instead of the existing one. This new layer includes 64 output channels, one input channel, a stride of 2.2, a padding of 3.3, and no bias. The kernel size is 7.7. The following layers have taken the place of the last layer, the fully connected layer (FC): Linear (2048, 512), ReLu, Dropout (0.2), Linear (512, 2), and a softmax layer. These fuzzy c layers aid with categorization. We optimized using the cross-entropy loss metric and the SGD optimizer with a learning rate of 0.001. Furthermore, the data needs to be processed in Numpy format. As shown in Algorithm 1.

Algorithm 1: Modification of the Initial Convolution Layer

```
# Import the necessary libraries and modules
import torch
import torch. nn as nn
import torch. optim as optim
from torchvision.models import resnet101

# Load the pre-trained ResNet-101 model
model_transfer = resnet101(pretrained=True)

# Modify the initial convolutional layer
model_transfer.conv1 = nn.Conv2d(
    in_channels=3,
    out_channels=64,
    kernel_size=(7, 7),
    stride=(2, 2),
    padding=(3, 3),
    bias=False
```

```
)

# Define a new classifier
classifier = nn.Sequential(
    nn.Linear(2048, 512),
    nn.ReLU(),
    nn.Dropout(0.2),
    nn.Linear(512, 2),
    nn.Softmax(dim=1)
)

# Replace the fully connected layer of the ResNet-101 model with the new classifier
model_transfer.fc = classifier

# Define the loss function
cel = torch.nn.CrossEntropyLoss()

# Configure the optimizer
optimizer = optim.SGD(model_transfer.parameters(), lr=0.001)
```

C. Inverse Regression of the ResNet-101 Network

1. **Objective Setting:** Five of the seven pivotal locations on the necessary slice correspond to the mandibular bone line and two to the mandibular nerve canals. This network was built to identify these points.
2. **Training Regimen:** The network is trained using previously tagged data to identify these seven sites.
3. **Post-Training Analysis:** Following training, the mandibular bone line and the mandibular bone's perpendicular intersection zone are identified using the network's capabilities.

In Algorithm 2, A regression task is the main topic of the second section. We used the novel ResNet-101 architecture. The proper MRI slice found in the first step serves as the input for this network. The model produces 14 output classes. Each class offers a value corresponding to a point's x or y coordinates for seven points. Changes were made to the classification layer, just like in the first phase. However, this time, the goal of the following linear layer is to produce 14 classes, each with distinct x and y coordinates.

Algorithm 2: Modification of the classification layer

```
# Import the necessary libraries and modules
import torch
import torch. nn as nn
import torch. optim as optim
from torchvision.models import resnet101

# Load the pre-trained ResNet-101 model
model_transfer = resnet101(pretrained=True)

# Modify the initial convolutional layer
model_transfer.conv1 = nn.Conv2d(
    in_channels=3,
    out_channels=64,
    kernel_size=(7, 7),
    stride=(2, 2),
    padding=(3, 3),
    bias=False
)
```

```

# Define a new classifier
classifier = nn.Sequential(
    nn.Linear(2048, 512),
    nn.ReLU(),
    nn.Dropout(0.2),
    nn.Linear(512, 14)
)

# Replace the fully connected layer of the ResNet-101 model with the new classifier
model_transfer.fc = classifier

# Define the loss function
cel = torch.nn.CrossEntropyLoss()

# Configure the optimizer
optimizer = optim.Adam(model_transfer.parameters(), lr=0.001)
```

D. Thickness Analysis at the Third Stage:

1. Computation of Thickness: Algorithms were created to accurately quantify the thickness of the mandibular cortical bone by utilizing data from earlier stages and comparing the results to a predefined "ground truth."

2. Analysis of Bone Intersections: Perpendicular bone intersections were computed using a deterministic function. After accounting for variations in density, these intersections provided data on bone thickness.

Finding the mandibular bone segment cut in the second stage is the first task of the third stage. We'll then gauge the sliced bone's thickness. The thickness of the bone is shown by the difference between the two specific spots that this code attempts to detect. The variables "int1" and "int2" hold these points. We can measure different bone thicknesses in different regions since bone thickness varies by region. The sections of the bone that are thickest and weakest can then be identified by comparing these measures. As shown in Algorithm 3.

Algorithm 3: Identifying Boundary Points

```
def GetDIFF(im):
    # Rotate the input image 270 degrees counterclockwise
    im = np.rot90(im, k=3)

    # Initialize lists to store boundary points
    ind1 = list()
    ind2 = list()

    # Find all potential points
    for i, colmn in enumerate(im):
        if sum(colmn) != 0:
            region = deepcopy(colmn)
            ind1.append((np.argmax(colmn), i))  # (i, im.shape[1]-np.argmax(colmn))
            region[np.argmax(colmn)] = 1
            ind2.append((np.arcmin(region), i))
```

3. Results

A. Fractal Analysis

The analyses were conducted after ensuring that the age, height, and weight data from the FD analysis followed a normal distribution using the Shapiro-Wilk and Cochran tests. The student t-test was utilized for variables that met the homoscedasticity and normalcy assumptions; the non-parametric Mann-Whitney test was applied for variables that did not. correlation coefficients were calculated to verify the hypothesized connections between the variables. We used the receiver operating characteristic (ROC) curve analysis to check if the FD measurement data was accurate across all ROIs, as shown in Figure 6. As initially proposed, the area under the ROC curve (AUC) was determined to compare the approaches' efficacy.33 The accuracy of FD measures in diagnosing osteoporosis was computed using the correct cutoffs.

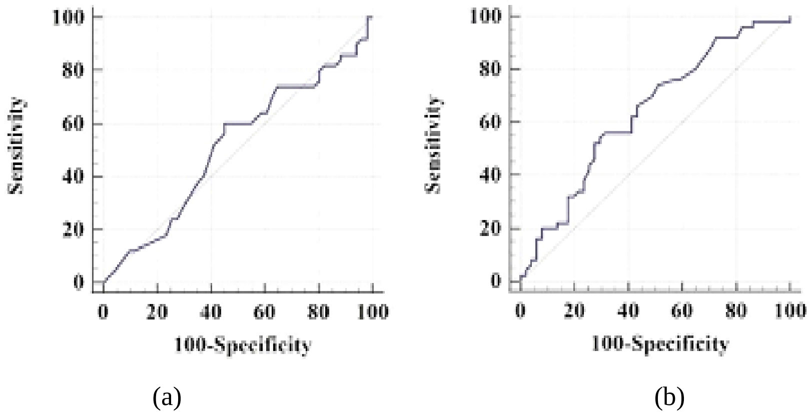

Figure 6: The receiver operating characteristic (ROC) curves of the fractal dimension analysis are at vertebral (a) and mandibular (b) locations.

A coefficient of repeatability equal to twice the standard deviation of the differences between the measurements was obtained by evaluating the consistency of the FD estimations using the Bland and Altman method [34]. This aimed to ensure that both the internal and external observers agreed. Using this metric, we found that the measurement precision ranged from 10% (excellent), 10% (good to moderate), and 20% (poor). Table 2 compares and contrasts the demographic and clinical characteristics of postmenopausal women with and without osteoporosis. Table 3 provides Correlation coefficients between fractal dimension measurements and bone mineral density at the lumbar spine, femoral neck, and total hip.

Table 2: Comparing postmenopausal adults with standard bone mineral density and osteoporosis using descriptive data means

Variables	Normal BMD	Osteoporosis
BMD L1-L4 (g/cm^2)	1.202±0.131	0.797±0.064**
BMD FN (g/cm^2)	1.022±0.116	0.765±0.101*
BMD TH (g/cm^2)	1.075±0.109	0.789±0.125*
FD ROI-v	1.80±0.17	1.80±0.18
FD ROI-m	1.76±0.23	1.65±0.26**
Age (years)	64.85±9.78	63.94±9.95
Height (cm)	157.73±7.32	151.73±6.34**
Weight (kg)	73.21±10.85	59.07±10.71*

Bone mineral density, or BMD TH, stands for whole hip, L1 for first lumbar vertebra, L4 for fourth cervical vertebra, FD for fractal dimension, and FN for femoral neck. ROI-m: area of interest in the panoramic reconstruction image of the mandible; ROI-v: region of interest in the second vertebra. **: $P<0.05$ by the Mann-Whitney test, *: $P<0.05$ by the t-test.

Comparing women who have undergone menopause and have normal BMD, the osteoporotic group exhibited significantly lower mean values for height and weight and BMD at all three locations for bones and FD at the mandibular site (ROI-m). There was a discernible statistical gap here. The mean values of FD at the vertebral location did not differ significantly between the two groups when statistical analysis was used to compare them. Regarding the amount of agreement amongst observers, most readings came in the margins of agreement (2SD).

When comparing the ROI-v and ROI-m, the mean difference was -0.02 (95% ranges of agreement: -0.19 to 0.16), and the mean difference when comparing the ROI-m and ROI-v was -0.07 (95% limits of agreement: -0.63 to 0.49) respectively. Results showed that ROI-m had 35% accuracy, but ROI-v was just 9% accurate.

When examining the level of agreement amongst observers, most measurements were within the standard deviation of the mean (2SD). Average measurement discrepancies for ROI-v were -0.2 (95% limits of agreement: -0.45 to 0.86), and for ROI-m, they were -0.31 (95% ranges of agreement: -1.05 to 0.41). Both ROIs, ROI-v (44% accuracy) and ROI-m (55% accuracy), performed worse than the precision of the intra-observer values. Patients' age, weight, and height were not observed to be associated with FD analyses (ROI-v and ROI-m; P>0.05). Table 3 demonstrates that when the proposed method was used for FD studies of the vertebral and mandibular sites, no correlation was found with BMD measurements of the lumbar spine, FN, or TH.

Table 3: Correlation coefficients between fractal dimension measurements and bone mineral density at the lumbar spine, femoral neck, and total hip

BMD L1-L4	BMD FN	BMD TH	p-value
ROI-v	- 0.075*	- 0.145*	- 0.0103*
ROI-m	0.059*	0.058*	0.059*

In contrast to ROI-m's 0.644 (P = 0.008), ROI-v's AUC was 0.531 (P = 0.720). Figure 5a shows the receiver operating characteristic (ROC) curve for ROI-v, while Figure 5b shows the ROC curve for ROI-m. Using a cutoff FD of 1.703 for the mandibular ROI, we found a sensitivity of 65.1%, specificity of 71.1%, positive predictive value of 65.1%, and negative predictive value of 61.7%.

B. Modular Neural Networks

The initial step was building a classification network based on ResNet-101 to identify the appropriate CBCT scan slice that displays the whole mandibular canal. Figure 7 illustrates that the training process reached its peak accuracy of 98.85% at the 39th epoch, whereas Figure 8 illustrates that the validation phase's accuracy of 93.99% was attained at the 35th epoch.

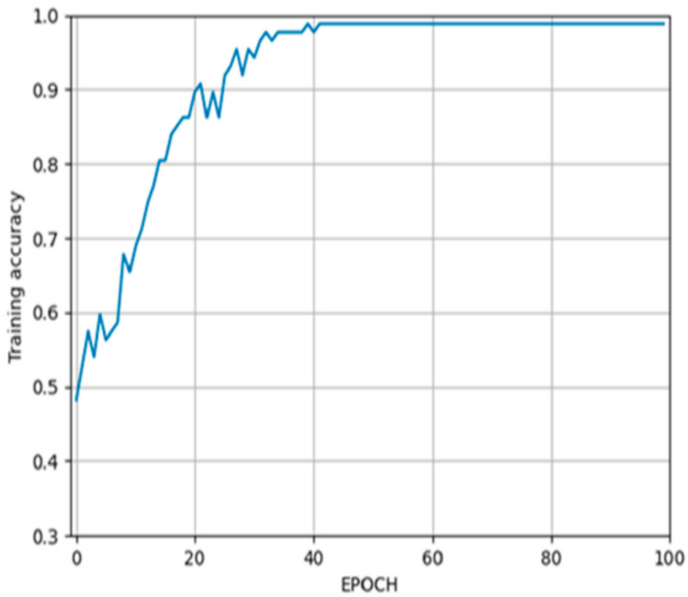

Figure 7: The accuracy of the training process

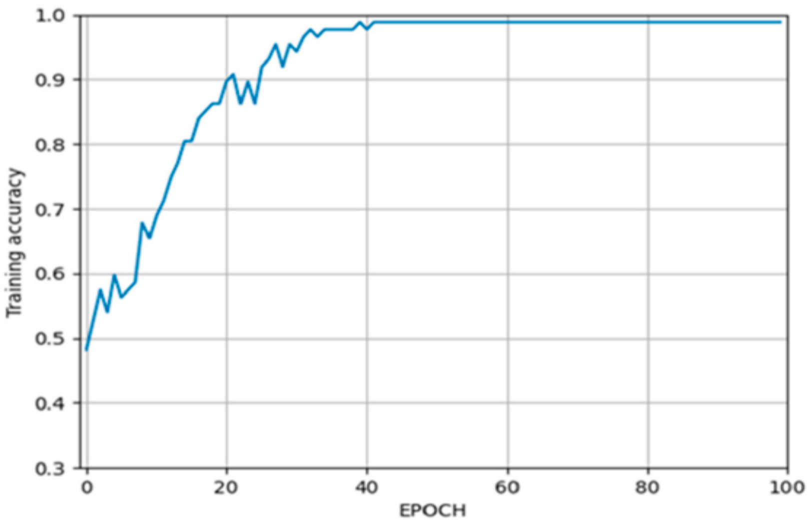

Figure 8: The accuracy of the validation process

The ResNet deep neural network was trained using the Stochastic Gradient Descent (SGD) optimizer with a learning rate (LR) 0.001. Training and validation sets were randomly selected from the dataset using a 70:30 ratio. The second phase involved training a regression network based on ResNet-101 to create two lines: one connecting the two points that made up the canal and the other drawing a line with five points across the mandibular bone. The training process's least L1 loss, which gauges how well the actual and projected points match, was 1.86 pixels (px) at the 30th epoch, as shown in Figure 9. The validation process's most minor loss was 1.02 pixels at the 70th epoch, as shown in Figure 10.

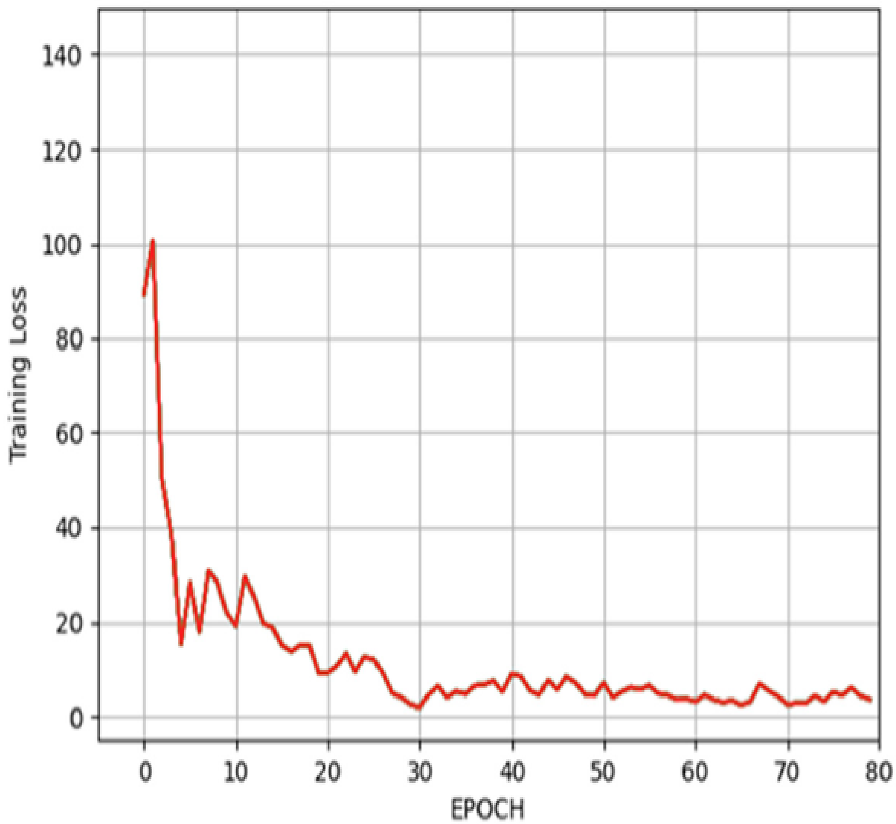

Figure 9: The training process's L1 loss (mean absolute error).

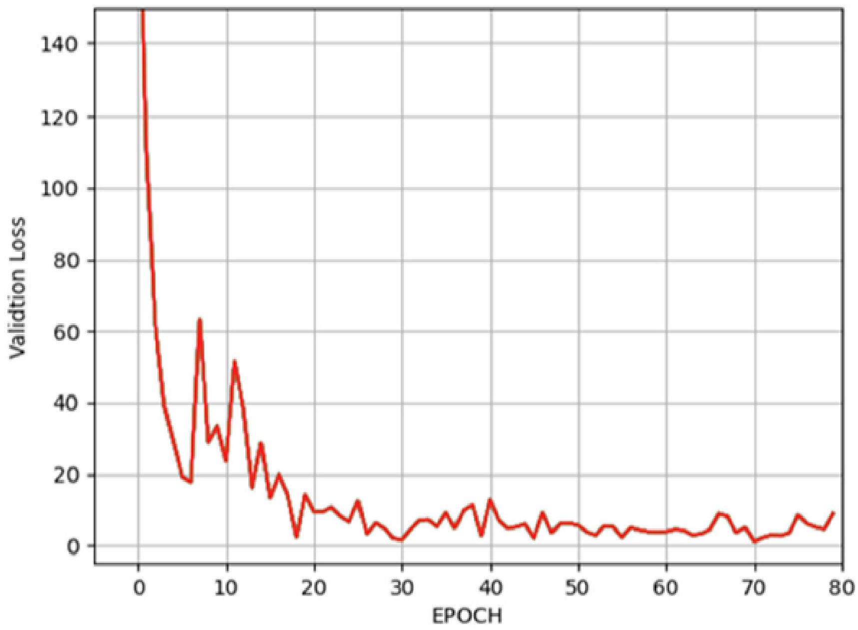

Figure 10: The L1 loss (mean absolute error) of the validation process

This step involves training the ResNet deep neural network with a learning rate 0.00 and the Adam optimizer. The values of pixels are multiplied by a conversion ratio of 0.3 to translate them to millimeters. The last step was developing an algorithm to evaluate the cortical thickness of the mandible bone to determine whether osteoporotic changes are present or absent in a particular CBCT slice.

Mandible bone thickness was calculated using a mean squared error (MSE) of 0.8377, with an average value of 0.018080 mm. Since not all patient data had been labeled, 180 observations of mandibular bone thickness were used in Stage 3. With a mean value of 2.9712 mm, the absolute mandibular bone thickness had a standard deviation (SD) of 0.9609 mm.

4. Conclusion

It has been demonstrated that women with osteoporosis have lower FD values on the trabecular bone of the jaw than do those without the condition. Despite this, there were no appreciable variations in the vertebrae's depth, width, or height. More accuracy and consistency might have been achieved in the findings of FD calculation tests used to identify postmenopausal women with low bone mineral density (BMD). This study also showed that deep convolutional neural networks (DCNNs) can diagnose osteoporosis from the mandibles' cone-beam computed tomography (CBCT) images. It employed a DCNN based on the ResNet-101 architecture to evaluate the CBCT scans of 188 patients.

The study's limitations, including the lack of literature on FD utilizing CBCT, emphasize the necessity of conducting more thorough studies on the image-processing methods, FD measurement procedures, and FD assessment zones that are part of the FD calculation strategy. The results validate the current study's conclusions, which indicate that densitometric inquiry is necessary for postmenopausal women and that FD analysis at the spinal site cannot be used as a stand-alone technique [34].

Even though a three-dimensional imaging modality on CBCT was used, the bone texture parameter (FD) was evaluated in two dimensions on multiplanar reconstruction pictures, similar to regular radiographs aside from soft tissue overlap. It is suggested that three-dimensional measuring software be used in future studies on the microstructural characteristics of bone. It's also critical to standardize the image processing technique. The ultimate goal is to enhance patient care by precisely and promptly detecting osteoporosis. Consequently, the modular approach can enhance the AI system's explainability and facilitate a more thorough DCNN training procedure. It is, therefore, a worthwhile topic for additional research.

Funding: “This research received no external funding.”

Conflicts of Interest: “The authors declare no conflict of interest.”

References

[1] NIH Consensus Development Panel on Osteoporosis Prevention, Diagnosis, and Therapy. Osteoporosis prevention, diagnosis, and therapy. JAMA, 285, 785-95, 2001.
[2] Atik OS, Gunal I, Korkusuz F, Burden of osteoporosis. Clin Orthop Relat Res, 443: 19-24, 2006.
[3] Marinho BC, Guerra LP, Drummond JB, Silva BC, Soares
[4] MM. The burden of osteoporosis in Brazil. Arq Bras Endocrinol Metabol, 58, 434-43, 2014.
[5] Høiberg MP, Rubin KH, Hermann AP, Brixen K, Abrahamsen
[6] B. Diagnostic devices for osteoporosis in the general population: a systematic review. Bone, 92, 58-69, 2016.
[7] Nakamoto T, Taguchi A, Ohtsuka M, Suei Y, Fujita M, Tanimoto K, et al. Dental panoramic radiograph as a tool to detect postmenopausal women with low bone mineral density: un-trained general dental practitioners' diagnostic performance. Osteoporos Int , 14, 659-64, 2003.
[8] Schuit SC, van der Klift M, Weel AE, de Laet CE, Burger H, Seeman E, et al. Fracture incidence and association with bone mineral density in older men and women: the Rotterdam Study. Bone, 34, 195-202, 2004.
[9] Sanchez-Molina D, Velazquez-Ameijide J, Quintana V, Arregui-Dalmases C, Crandall JR, Subit D, et al. Fractal dimension and mechanical properties of human cortical bone. Med Eng Phys, 35, 576-82, 2013.
[10] Shokri A, Ghanbari M, Maleki FH, Ramezani L, Amini P, Tapak L, Relationship of gray values in cone beam computed tomography and bone mineral density obtained by dual-energy X-ray absorptiometry. Oral Surg Oral Med Oral Pathol Oral Radiol, 128, 319-31, 2019.
[11] Pachêco-Pereira C, Almeida FT, Chavda S, Major PW, Leite A, Guerra EN, Dental imaging of trabecular bone structure for systemic disorder screening: a systematic review. Oral Dis, 25, 1009-26, 2019.
[12] Lespessailles E, Gadois C, Kousignian I, Neveu JP, Fardel-Lone P, Kolta S, et al. The clinical interest of bone texture analysis in osteoporosis: a case-control multicenter study. Osteoporos Int, 19, 1019-28, 2008.
[13] Guenoun D, Le Corroller T, Acid S, Pithioux M, Pauly V, Ariey-Bonnet D, et al. Radiographical texture analysis improves the prediction of vertebral fracture: an ex vivo biomechanical study. Spine (Phila Pa 1976) 38, E1320-6, 2013.
[14] Le Controller T, Halgrin J, Pithioux M, Guenoun D, Chabrand P, Champsaur P, Combination of texture analysis and bone mineral density improves the prediction of fracture load in human femurs. Osteoporos Int, 23,163-9, 2012.
[15] Mahmoud A. Zaher, Nabil M. Eldakhly, Yahia B. Hassan, The Emerging Role of Wearable Health Technologies in Proactive Disease Prevention, International Journal of Wireless and Ad Hoc Communication , Vol. 8 , No. 1 , (2024) : 40-50 (Doi : https://doi.org/10.54216/IJWAC.080105)
[16] Yaşar F, Akgünlü F, The differences in panoramic mandibular indices and fractal dimension between patients with and without spinal osteoporosis. Dentomaxillofac Radiol, 35, 1-9, 2006.
[17] Tosoni GM, Lurie AG, Cowan AE, Burleson JA. Pixel intensity and fractal analyses: detecting osteoporosis in perimenopausal and postmenopausal women using digital panoramic images. Oral Surg Oral Med Oral Pathol Oral Radiol Endod, 102, 235-41, 2006.
[18] Mohamed Saber , El-Sayed M. El-Kenawy , Abdelhameed Ibrahim , Marwa M. Eid, Watermarking System for Medical Images Using Optimization Algorithm, Fusion: Practice and Applications, Vol. 10 , No. 1 , (2023) : 89-99 (**Doi :** https://doi.org/10.54216/FPA.100105)
[19] Bollen AM, Taguchi A, Hujoel PP, Hollender LG, Fractal dimension on dental radiographs. Dentomaxillofac Radiol, 30, 270-5, 2001.
[20] Law AN, Bollen AM, Chen SK, Detecting osteoporosis using dental radiographs: a comparison of four methods. J Am Dent Assoc, 127, 1734-42, 1996.
[21] Magat G, Ozcan Sener S, Evaluation of a trabecular pattern of the mandible using fractal dimension, bone area fraction, and grayscale value: comparison of cone-beam computed tomography and panoramic radiography. Oral Radiol, 35, 35-42, 2019.
[22] Bornstein M, Scarfe W, Vaughn V, Jacobs R, Cone beam computed tomography in implant dentistry: a systematic review focusing on guidelines, indications, and radiation dose risks. Int J Oral Maxillofac Implants, 29 Suppl, 55-77, 2014.
[23] Yepes JF, Al-Sabbagh M, Use of cone-beam computed tomography in early detection of implant failure. Dent Clin North Am, 59, 41-56, 2015.
[24] Brasileiro CB, Chalub LL, Abreu MH, Barreiros ID, Amaral TM, Kakehasi AM, et al., Use of cone beam computed tomography in identifying postmenopausal women with osteoporosis, Arch Osteoporos, 12- 26, 2017.
[25] Alkhader M, Aldawoodyeh A, Abdo N. Usefulness of measuring the bone density of mandibular condyle in patients at risk of osteoporosis: a cone beam computed tomography study. Eur J Den, 12, 363-8, 2018.

[26] Guerra EN, Almeida FT, Bezerra FV, Figueiredo PT, Silva MA, De Luca Canto G, et al. The capability of CBCT to identify patients with low bone mineral density: a systematic review. Dentomaxillofac Radiol, 46, 20160475, 2017.
[27] De Castro JG, Carvalho BF, de Melo NS, de Souza Figueiredo PT, Moreira-Mesquita CR, de Faria Vasconcelos K, et al., A new cone-beam computed tomography-driven index for osteoporosis prediction. Clin Oral Investig, 24, 3193-202, 2020
[28] Mostafa RA, Arnout EA, Abo El-Fotouh MM, Feasibility of cone beam computed tomography radiomorphometric analysis and fractal dimension in assessment of postmenopausal osteoporosis in correlation with dual X-ray absorptiometry. Dentomaxillofac Radiol, 45, 20160212, 2016.
[29] Güngör E, Yildirim D, Çevik R, Evaluation of osteoporosis in jaw bones using cone beam CT and dual-energy X-ray absorptiometry. J Oral Sci, 58, 185-94, 2016.
[30] Hilton C, Milinovich A, Felix C, Vakharia N, Crone T, Donovan C, Proctor A, Nazha A, Personalized Predictions of Patient Outcomes during and after Hospitalization Using Artificial Intelligence. NPJ Digit. Med., 3, 51, 2020.
[31] Dlamini Z, Francies F. Z., Hull R., Marima R, Artificial Intelligence (AI) and Big Data in Cancer and Precision Oncology. Comput.Struct. Biotechnol. J., 18, 2300–2311, 2020.
[32] Cavalcante D.D.S., Silva P.G.D.B., Carvalho F.S.R., Quidute A.R.P., Kurita L.M., Cid A.M.P.L., Ribeiro T.R., Gurgel M.L., Kurita B.M., Costa F.W.G, Is Jaw Fractal Dimension a Reliable Biomarker for Osteoporosis Screening? A Systematic Review and Meta-Analysis of Diagnostic Test Accuracy Studies. Dentomaxillofacial Radiol. , 51, 20210365, 2022.
[33] Xu W, Fu Y, Zhu D, ResNet and Its Application to Medical Image Processing: Research Progress and Challenges. Comput. Methods Programs Biomed, 240, 107660, 2023.
[34] Sindeaux R, Figueiredo PT, de Melo NS, Guimarães AT, Lazarte L, Pereira FB, et al. Fractal dimension and mandible-lar cortical width in average and osteoporotic men and women. Maturitas 77, 142-8, 2014.